Materials and Structures/Matériaux et Constructions, Vol. 33, April 2000, pp 147-153

SCIENTIFIC REPORTS

Microstructure and transport properties of porous building materials. II: Three-dimensional X-ray tomographic studies

D. P. Bentz[1], D. A. Quenard[2], H. M. Kunzel[3], J. Baruchel[4], F. Peyrin[4,5], N. S. Martys[1] and E. J. Garboczi[1]

(1) Building and Fire Research Laboratory National Institute of Standards and Technology Gaithersburg, MD 20899 USA – (2) Centre Scientifique et Technique du Batiment, 24 Rue Joseph Fourier, F-38400 Saint-Martin d'Heres, France – (3) Fraunhofer-Institut fur Bauphysik, IBP Postfach 11 52, D-83601 Holzkirchen, Germany – (4) ESRF, Grenoble, France – (5) CREATIS-INSA, Lyon, France

Paper received: April 14, 1999; Paper accepted: October 18, 1999

ABSTRACT

Three-dimensional X-ray microtomography is used to obtain three-dimensional images of the microstructure of two types of brick. The images are processed to remove the noise (random and circular pattern) and then thresholded to match the porosity determined experimentally. The 3-D binary images are then analyzed to estimate their vapor diffusivity and air permeability to compare to experimental data published in part one of this report. Care must be taken in obtaining the tomographic images at a resolution that both enables isolation and quantification of the pores of interest and provides a representative elementary volume for the transport property calculations. In general, the agreement between computed and measured properties is reasonable, suggesting that X-ray microtomography can provide valuable information on the characteristics and properties of the pore networks developed in these porous building materials. A preliminary evaluation indicates that the Katz-Thompson relationship between permeability, diffusivity, and pore size is valid for these materials.

RÉSUMÉ

La microtomographie à rayons X synchrotron est utilisée pour obtenir des images tridimensionnelles de la microstructure de deux types de briques. Les images sont tout d'abord traitées pour éliminer le bruit (anneaux aléatoires) et ensuite seuillées par ajustement avec la porosité déterminée expérimentalement. À partir des images binaires 3D, on estime numériquement la diffusivité à la vapeur et la perméabilité à l'air, les valeurs obtenues sont ensuite comparées avec les données expérimentales publiées dans la partie I de cette communication. Dans le cadre d'une telle procédure, la résolution des images doit à la fois rendre possible la discrimination et la quantification de tous les pores importants vis-à-vis du phénomène étudié et fournir un volume élémentaire représentatif pour le calcul des propriétés de transport. L'accord satisfaisant obtenu entre les valeurs calculées et mesurées montre que la microtomographie X peut fournir des informations pertinentes sur les caractéristiques et les propriétés du réseau poreux des matériaux de construction. Une évaluation préliminaire indique que la relation de Katz-Thompson entre la perméabilité, la diffusivité et la taille des pores est applicable pour ces matériaux.

1. INTRODUCTION

In part one of this study [1], a linkage was established between the pore structure and transport properties (sorptivity, diffusivity, and permeability) for a set of three common building materials. Using mercury intrusion porosimetry and scanning electron microscopy analysis in combination with two different types of computer models, computed transport properties based on the models compared favorably with those measured experimentally on the same suite of materials. In this present paper, this study is extended by directly analyzing the three-dimensional microstructure of two of the materials (bricks) as exemplified by X-ray microtomographic images obtained using beam line ID19 at the European Synchrotron Research Facilities (ESRF) in Grenoble, France. The two bricks examined are a lime silica brick formed by high pressure steam curing of a mixture of lime and silica, and a clinker brick which is a hard-burned clay brick. Both are typically used in the rain screens of cavity walls [1].

The 3-D images (256 pixels × 256 pixels × 256 pixels) are first processed to remove the random noise and the "circular ring" noise pattern often inherent in X-ray microtomographic images. The latter noise is characterized by a series of concentric rings radiating outward from the center of the sample in one of the image planes. After processing, the microstructures are binarized to

Editorial Note

Mr. D. P. Bentz is a RILEM Senior Member. He works at NIST (USA), a titular member. He is also a Member of RILEM Coordinating Committee. He was the 1998 Robert l'Hermite medallist.

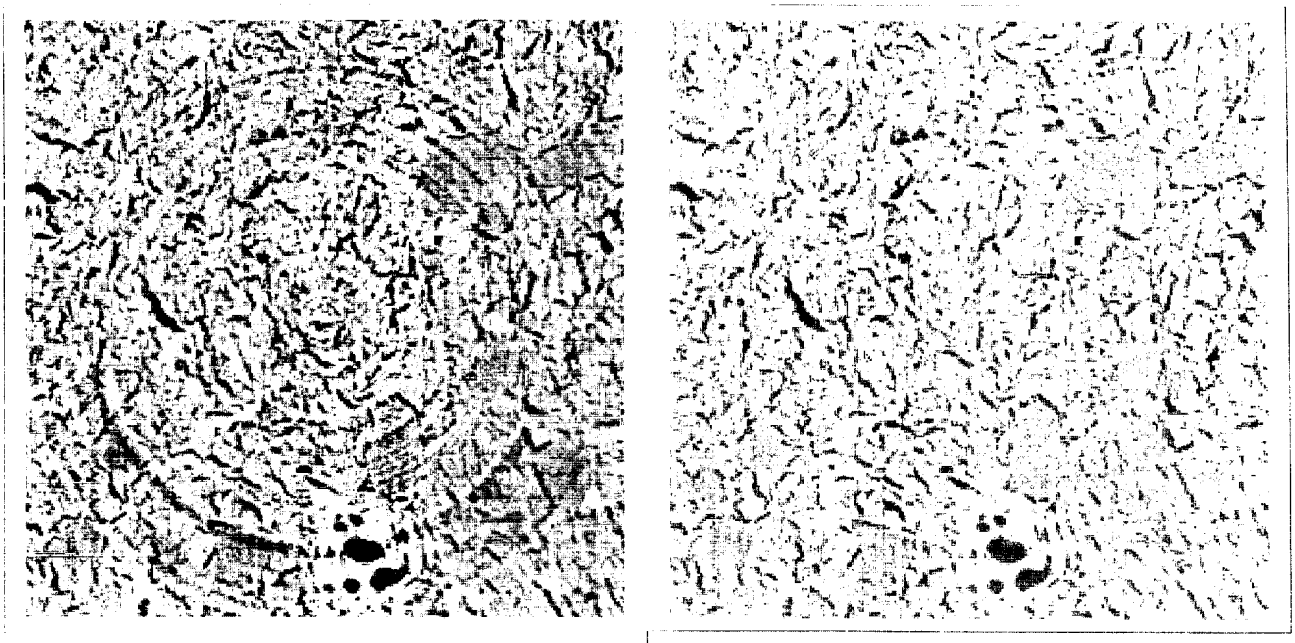

Fig. 1 – Original, processed, and binary images for the clinker brick. Thresholded porosity is 20%. Image size is 256 pixels × 256 pixels or 1.7 mm × 1.7 mm.

match the overall porosity measured experimentally on the materials. For one of the bricks, the clinker brick, this is accomplished via a simple thresholding operation. For the lime silica brick, however, because the microstructure contains multi-scale features (pores) which are not resolvable using the X-ray tomographic equipment, a multi-scale approach to assigning porosity and computing transport properties is applied [1, 2]. After binarization, 100 pixel × 100 pixel × 100 pixel or 200 pixel × 200 pixel × 200 pixel subsets of the resultant images are analyzed to compute diffusivities and permeabilities using previously developed techniques [1, 3-5]. These computed values are compared to those previously measured experimentally [1]. It should be noted that the computational programs are not limited to transport properties, as shrinkage and elastic response can also be simulated on any 3-D binary image of a porous media [6].

2. EXPERIMENTAL AND COMPUTATIONAL TECHNIQUES

2.1 Image acquisition

Within the last decade, X-ray computed microtomography (μCT) has become an important tool for investigation in materials science [7-9], biology, and medicine [10], since it is a non-destructive method which provides three-dimensional information.

In principle, X-ray microtomography is similar to the conventional scanners used in medical applications, except that it provides images with higher spatial resolution. Getting higher spatial resolution in reasonable acquisition times requires intense X-ray beams. For this purpose, the use of X-ray beams extracted from the synchrotron radiation is particularly well suited. In addition, synchrotron radiation offers the possibility to select monochromatic X-ray beams (within a small energy bandwidth) with an energy optimized for the sample under investigation, while at the same time maintaining a high enough photon flux rate for efficient imaging. Monochromaticity is of great interest in tomography since it avoids beam hardening artifacts, which occur when the low energy radiation of the beam is absorbed by the sample.

The samples were imaged on the 3-D μCT setup developed on beamline ID 19 at the ESRF. The system uses a large monochromatic parallel beam and a 2-D area detector. The sample to be imaged is mounted on a translation/rotation stage allowing precise alignment in the beam. The acquisition consists of recording radiographic images of the sample for different angular positions. After conversion to light by a fluorescent screen,

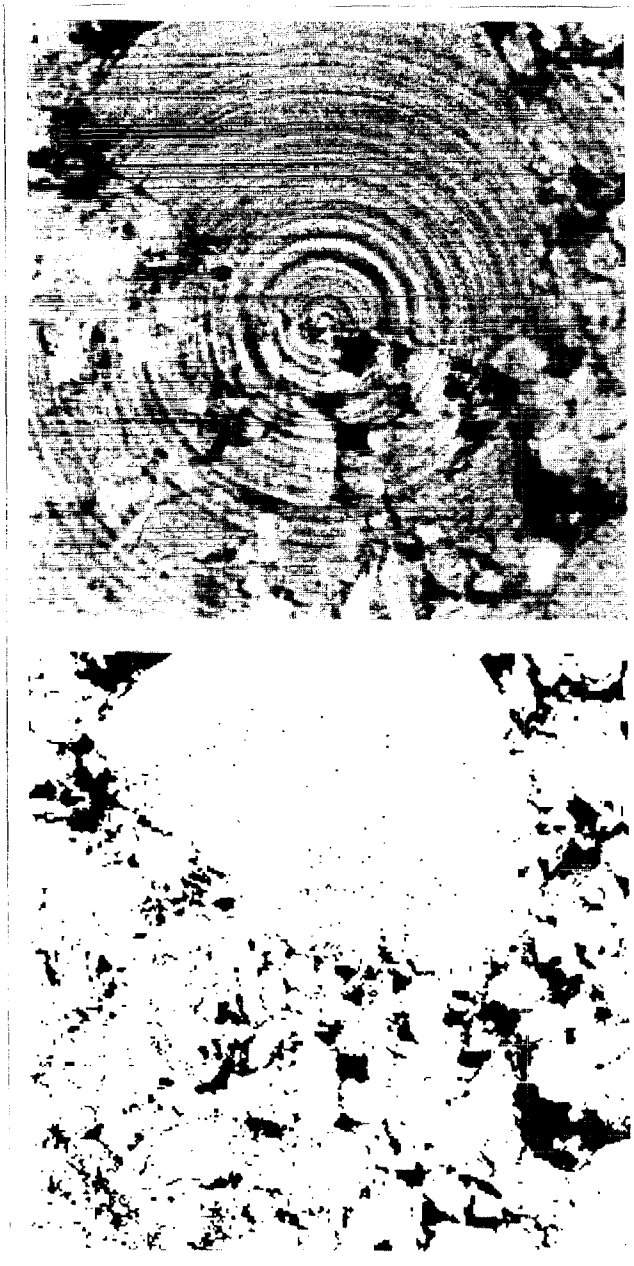

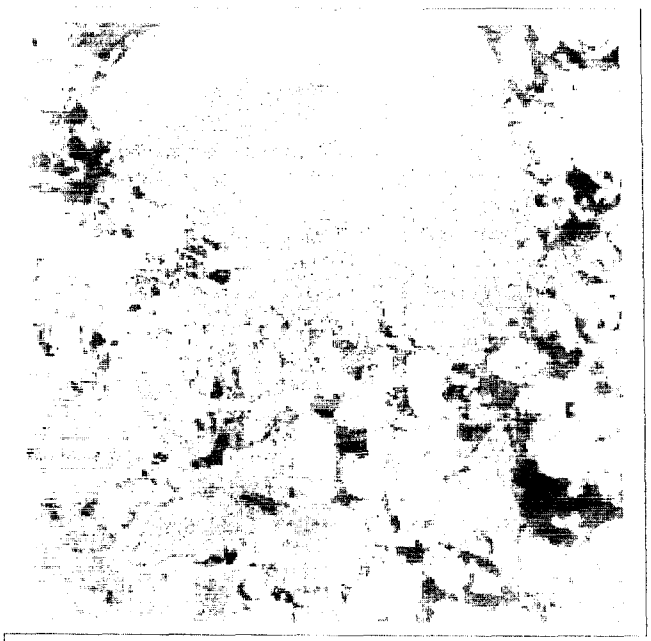

Fig.2 – Original, processed, and binary images for the lime silica brick. Thresholded porosity is 16%. Image size is 256 pixels × 256 pixels or 1.7 mm × 1.7 mm.

the radiographic images are digitized using a Frelon Camera [11], which consists of a 2-D CCD (Charge Couple Device) array with 1024 elements × 1024 elements, each 19 µm by 19 µm, and offers a dynamic range of 14 bits. The CCD camera is mounted perpendicularly to the X-ray beam in order to avoid direct interactions which cause noise in the recorded images. An optical magnification is used resulting in a pixel size of 6.65 µm by 6.65 µm for the recorded image. A 3-D filtered backprojection algorithm is then used to reconstruct a 3-D image of the sample from the series of 2-D projections [12].

In this experiment, the specimens were scanned using 25 keV X-rays. For each sample, 900 radiographic images were acquired over a field of view of 180 degrees. The 3-D reconstruction was limited to a 256 × 256 × 256 region of interest (ROI) within the sample.

2.2 Image processing

Two-dimensional slices extracted from the 3-D tomographic images are provided in the upper left portions of Figs. 1 and 2. From these images, it is clear that a predominant artifact is the circular ring pattern emanating from the central point. These artifacts result from dust on the monochromator surface. Attempts to remove these artifacts using median filtering [13] were only partially successful, resulting in images which could not be easily thresholded to obtain binary pore/solid representations. Thus, a more direct approach to removing this noise pattern was developed. Basically, our goal is to remove the variation in greylevel as we proceed from one radial distance to another, since it is this variation that is responsible for the observed ring pattern. Because of the concentric ring nature of this noise, a special filter function of the form:

$$g(x,y,z) = \left[g(x,y,z) - \overline{g_z(r)} \right] + 128 \qquad \begin{matrix} 255 \\ | \\ | \\ 0 \end{matrix} \qquad (1)$$

is applied in each z plane, where $g_z(r)$ is the average greylevel computed at each radial distance r in plane z and the result is limited to the range [0,255]. Originally, this filter was applied to each 2-D slice of the image in its entirety, but this resulted in the emergence of a new artifact due to the subtle greylevel variation in various quadrants of the image. Thus, each image plane was subdivided into four subquadrants ($x < 0$, $y < 0$; $x < 0$, $y > 0$; $x > 0$, $y < 0$; $x > 0$, $y > 0$) where ($x = 0$, $y = 0$) represents the central point of the image plane. The above function

was then applied separately in each quadrant. Finally, a 3-D median filter of size 5 pixels × 5 pixels × 5 pixels was applied to remove any remaining X-ray imaging artifacts and randomly distributed noise. As will be presented in the results section, this produced images of greatly enhanced contrast, where the ring artifacts were basically removed and no longer influenced the segmentation process.

From the previous study [1], the porosities of the two bricks were known experimentally. For the clinker brick, the processed 256 × 256 × 256 3-D image was thresholded to obtain a porosity of 20% and the central 100 × 100 × 100 and 200 × 200 × 200 portions were selected for further computations. For the lime silica brick, the threshold porosity was set at 16%, as determined previously for this coarser scale [1], with the remainder of the overall porosity being distributed at a finer scale within the solids (16% porosity also within the solids resulting in 0.16 + (1.-0.16)*0.16 = 0.294 total porosity). In this manner, the overall porosity is very close to the experimentally determined value of 30% [1].

2.3 Transport property measurement

The measurement of transport properties of these bricks has been described in detail previously [1]. Vapor diffusivity was measured by means of a cup test according to DIN standard 52-615 [14]. The relative humidity gradient for this test was between 3% RH and 50% RH. When the rate of mass increase of the cup containing the sample was linear, the slope was used to determine the material vapor diffusivity. Air permeability was measured on the same samples used in the vapor diffusivity test. The sample was sealed in the testing device and the air flow measured at a series of pressure steps. Knowing the flow rate and the pressure differential across the sample, the air permeability was easily calculated [1].

2.4 Transport property computations

To compute vapor diffusivity, both finite difference and finite element techniques [15] were applied to the 3-D digital 100 pixel × 100 pixel × 100 pixel binary images. The finite element techniques consider corner and edge connections as well as pixel face connections and thus result in higher computed values for relative diffusivity. Both techniques were executed because of the extreme fineness of the slit-like pores in the clinker brick images, as seen in Fig. 1. For pores this small, the overall connectivity of the pore system can be largely influenced by diagonal pixel connections in the 3-D image. To convert the relative diffusivities to absolute values, a value of 0.0922 m^2/h was used as the diffusivity of water vapor in air [16]. For the lime silica brick, relative diffusivities of 0.007 and 0.015 were assigned to the solid phases, corresponding to the values determined for the 16% porosity phase using the finite difference and finite element techniques, respectively. Thus, we are assuming that the lime silica brick has a self-similar microstructure such that the relative diffusivity computed for the coarse pores can be used to provide the values needed for the fine-scale porosity present in the "solids" in the 3-D μCT images.

To compute permeability, Stokes equation for slow incompressible flow was solved using a finite difference scheme along with non-centered difference equations [4, 5]. These calculations were performed on both 100 pixel × 100 pixel × 100 pixel and 200 pixel × 200 pixel × 200 pixel central portions of the 3-D microstructure to examine the effects of sample size (with respect to obtaining a representative elementary volume) on permeability. For the lime silica brick, no attempt was made to account for the contribution of the fine-scale porosity to the overall permeability, as it was considered that the measured permeability would be dominated by the porosity present at the coarser scale imaged by the X-ray tomography technique. In all cases, transfer coefficients were computed for each of the three principal directions.

3. RESULTS

3.1 Microstructure

Figs. 1 and 2 provide a series of 2-D images located at slice z = 100 from the 256^3 microstructures. In each image set, the upper left image is the as received data, the upper right shows the image after the filtering process, and the lower left image provides the resultant image after the binarization process. In both cases, the large improvement in image quality obtained via the filtering process is clearly evident. To the viewer's eye, the segmentation into porosity and solid provided in the binary image appears quite reasonable at the assigned porosities of 20% and 16%, for the clinker and lime silica bricks, respectively. While the pore space appears disconnected in the two-dimensional images, the 3-D binary images shown in Fig. 3 clearly illustrate that the porosity is percolated for both bricks. These 3-D images (50 pixel × 50 pixel × 50 pixel) illustrate the central portions of the 3-D microstructures which were selected for computation of the materials' transfer coefficients.

3.2 Measured and computed transport properties

The computed and measured transport properties are summarized in Table 1. In general, the agreement between experimental and computed transfer coefficients is reasonable, but for both bricks, further improvements could be expected by changing the resolution at which the X-ray microtomographic images were acquired.

For the clinker brick, the volume imaged in the 256 × 256 × 256 array is greater than needed to be representative of the microstructure. For this material, the problem is that the individual slit-like pores are very

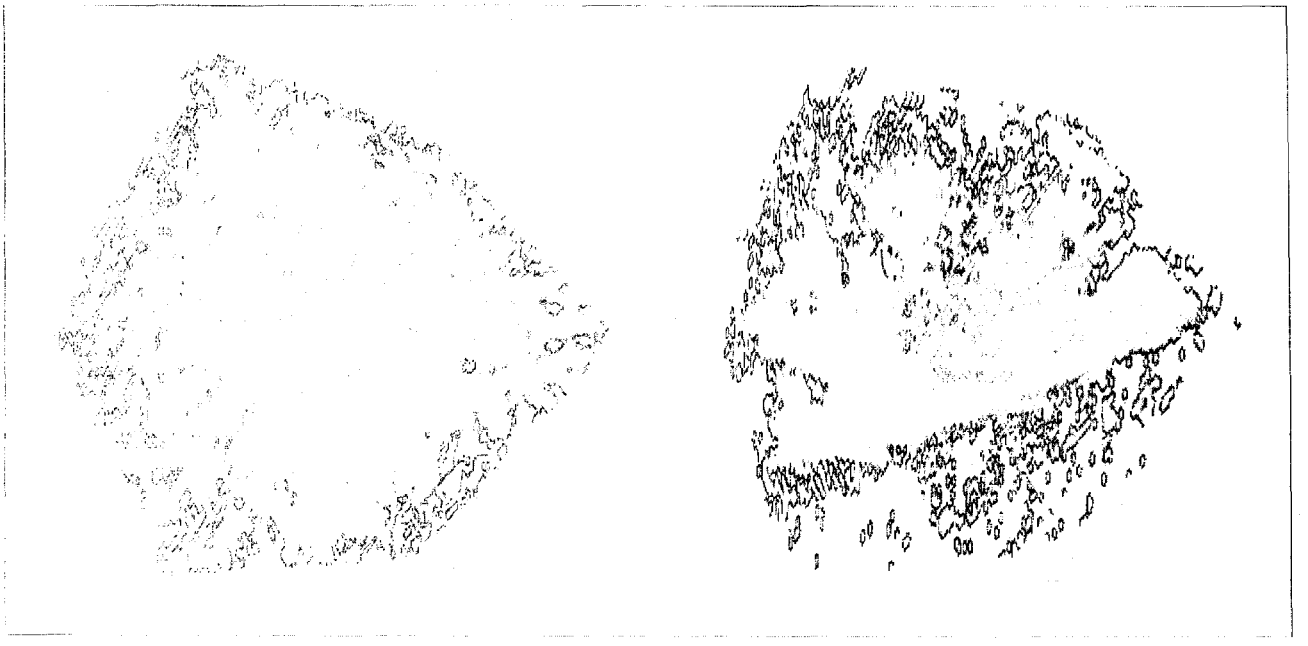

Fig. 3 – 3-D binary images of clinker (top) and lime silica (bottom) bricks. Images are 50 pixels × 50 pixels × 50 pixels in size from the central portion of each microstructure.

small and are typically only one to three pixels in width. Thus, the connectivity of the 3-D image is less than that of the original microstructure, and this system would benefit from an increase in resolution in the μCT data set. This can be clearly seen in the results where the vapor diffusivities computed using the finite element (more connected) computation are much greater and much closer to the experimental values than those determined using finite differences. In fact, the overall average of the finite difference and finite element values, 0.0016, is within 20% of the measured value, a reasonable agreement. One can also note a high degree of anisotropy in the sample microstructure as evidenced by the ratio of 2 to 3 between minimum and maximum values for the transfer coefficients computed in each of the three principal directions.

In terms of permeability, the computed values are on the average a factor of 3 too high in comparison to the single experimental value. Some of this variation could be due to the anisotropy present in this material. In hindsight, it would have been very useful to experimentally measure the transfer coefficients of this material in each of the three principal directions. The computed permeability values are also likely too high due partially to the resolution problem. Because the smallest resolvable pores are 6.65 μm (1 pixel) in size and permeability scales as pore diameter squared [17], if 4 μm pores were instead the true characteristic feature of the microstructure, the computed permeabilities would be a factor of $(6.65/4)^2 = 2.76$ too high, very close to the observed average ratio of computed to experimental values. Once again, an increase in the μCT data set resolution, such that the pores were on average at least 3 pixels wide, would be beneficial.

For the lime silica brick, conversely, the pores are quite large and well delineated in the 3-D image. In this case, the problem is one of obtaining a large enough image to provide a representative elementary volume for the heterogeneous microstructure, as the microstructure in Fig. 2 is dominated by the presence of a single large grain in the image's upper central region. Fortunately, the vapor diffusivity results are fairly insensitive to system size, and all computed values agree fairly well with the single measured value of diffusivity (the overall average computed value being within 2% of the experimental one). Because the pore space is very well connected in the 3-D image for the lime silica brick, there is a much smaller difference between the values provided by

Table 1 – Measured and computed transport properties for bricks

Property	Clinker brick	Lime silica brick
Total porosity (%)	20	30
Measured Vapor Diffusivity (m^2/h)	0.002	0.004
Computed Vapor Diffusivity (m^2/h)a	0.0003,0.0005,0.0007	0.0032,0.0022,0.0027
Computed Vapor Diffusivity (m^2/h)b	0.0020,0.0027,0.0036	0.0053,0.0044,0.0058
Measured Air Permeability (μm^2)	0.006	0.039
Computed Air Permeability (μm^2)c	0.024,0.008,0.013	0.062,0.17,0.027
Computed Air Permeability (μm^2)d	0.032,0.011,0.019	0.11,0.23,0.088

a - Computed using finite difference technique.
b - Computed using finite element technique.
c - Computed on a 100 × 100 × 100 image.
d - Computed on a 200 × 200 × 200 image.

the finite difference and finite element techniques than for the clinker brick.

For permeability, in an attempt to obtain a representative elementary volume, computations were performed on both the central 100 × 100 × 100 and 200 × 200 × 200 portions of the 3-D microstructure. As can be seen in Table 1, little change was observed in going to the larger systems, suggesting that in this case, the X-ray microtomographic data really needs to be acquired at a lower resolution (larger sample volume) to provide a more representative 3-D image for computing permeability for this brick. On average, the computed values are a factor of about 3 too high in comparison to the single experimental value, which was obtained on a much larger sample area (100 cm^2 vs. 0.029 cm^2 for the 256 pixel × 256 pixel tomographic images).

3.3 Katz-Thompson relationship in bricks

The data set generated for the bricks allows us to quantitatively evaluate the use of the Katz-Thompson relationship for predicting the permeability of these porous materials. The basic Katz-Thompson relationship is given by [18]:

$$k = \frac{\frac{D}{D_0} * D_c^2}{226} \qquad (2)$$

where k is the permeability, D/D_0 is the relative diffusivity, and D_c is the critical pore diameter evaluated from a mercury intrusion experiment and corresponding to the largest pore size for which there exists a connected pathway through the microstructure when considering only pores of this size and larger.

Experimentally, permeability has been measured and the relative diffusivity can be obtained by dividing the measured value by the value for water vapor in air (0.0922 m^2/h). However, a measure of D_c is lacking. But, computationally, the 3-D microstructural binary images can be evaluated to provide an estimate of D_c in the following manner. First, the connectivity of the systems can be examined using a "burning" algorithm [19] to determine the fraction of the overall porosity which is part of a connected pathway through the microstructure for a "diameter" of one pixel. For the clinker brick and lime silica bricks, we find percolated fractions of 0.78 and 0.85, respectively. In addition, a program which simulates the 3-D intrusion of spherical particles of various sizes can be used as a coarse simulation of the mercury intrusion process (coarse because in three dimensions, the intruding mercury surface is characterized by two radii of curvature and may not be spherical) [4]. For a D_c = 3 pixels (about 20 μm), the pores in the clinker brick are virtually inaccessible, while about 25% of those in the lime silica brick are accessible when intruding from one surface of the 3-D system. Thus, reasonable estimates of D_c might be 1 pixel (6.65 μm) and 2 pixels (13.3 μm) for the clinker and lime silica bricks, respectively. These values are in good agreement with mercury intrusion porosimetry curves presented previously [1]. Substituting these values into equation 2 along with the measured relative diffusivities, one computes estimated permeabilities of 0.004 μm^2 for the clinker brick and 0.034 μm^2 for the lime silica brick, in good agreement with the experimentally determined values. This preliminary analysis indicates that the Katz-Thompson relationship very likely holds for these bricks, as well as for the porous rocks to which it was originally applied [18]. Here again, the analysis for the clinker brick would benefit from having a data set obtained at a higher resolution to allow a more accurate determination of D_c for this material.

4. CONCLUSIONS

X-ray microtomography can provide valuable three-dimensional images of the microstructure of porous building materials, but the chosen resolution of the images must be carefully selected to balance pore size and representative elementary volume concerns. Too high a resolution provides excellent individual pore delineation, but results in an overall volume which is too small to be representative. Too low a resolution provides a good representative elementary volume, but may result in pores which are difficult to isolate and whose 3-D connectivity is less than the pores in the actual material. For a material with a wide range of pore sizes (such as cement paste or mortar), it will be extremely difficult to balance these two concerns and a multi-scale approach, such as that used for computing the diffusivity of the lime silica brick in this study, may be needed to produce quantitative comparisons to experimental data. When these concerns are properly balanced, or at least considered in the subsequent computations of transport properties, the computed transfer coefficients compare favorably with their experimental counterparts. Experimentally, if it is suspected that a material may be anisotropic, transfer coefficients should be measured in each of the three principal directions to test this hypothesis. Finally, it has been demonstrated that the Katz-Thompson relationship can be used to characterize the transport properties and pore sizes of the bricks examined in this study.

ACKNOWLEDGEMENTS

Portions of this study were conducted as part of the European Science Project CT 91-0737, entitled "Characterization of Microstructure as a Tool for Prediction of Moisture Transfer in Porous Media."

REFERENCES

[1] Quenard, D. A., Xu, K., Kunzel, H. M., Bentz, D. P. and Martys, N. S., 'Microstructure and transport properties of porous building materials', *Mater. Struct.* **31** (209) (1998) 317–324.

[2] Bentz, D. P., Garboczi, E. J. and Lagergren, E. S., 'Multi-scale microstructural modelling of concrete diffusivity: Identification of significant variables', *Cem. Concr. Agg.* **20** (1) (1998) 129–139.

[3] Garboczi, E. J. and Bentz, D. P., 'Computer simulation of the diffusivity of cement-based materials', J. Mater. Sci. **27** (1992) 2083–2092.

[4] Schwartz, L. M., Martys, N. S., Bentz, D. P., Garboczi, E. J. and Torquato, S., 'Cross property relations and permeability estimation in model porous media', *Phys. Rev. E* **48** (6) (1993) 4584–4591.

[5] Bentz, D. P. and Martys, N. S., 'Hydraulic radius and transport in reconstructed model three-dimensional porous media', *Transport in Porous Media* **17** (3) (1994) 221–238.

[6] Bentz, D. P., Garboczi, E. J. and Quenard, D.A., 'Modelling drying shrinkage in reconstructed porous materials: Application to porous Vycor glass', *Modell. Simul. Mater. Sci. Eng.* **6** (1998) 1–26.

[7] Flannery, B. P., Deckman, H. W., Roberge, W. G. and D'Amico, K. L., 'Three-dimensional X-ray microtomography', *Science* **237** (1987) 1439–1443.

[8] Spanne, P., *et al.*, 'Synchrotron computed microtomography of porous media: Topology and transports', *Phys. Rev. Letters* **73** (8) (1994) 2001–2004.

[9] Bentz, D. P., Martys, N. S., Stutzman, P. E., Levenson, M. S., Garboczi, E. J., Dunsmuir, J. and Schwartz, L. M., 'X-ray microtomography of an ASTM C109 mortar exposed to sulfate attack', *MRS Symposium Proceedings* **370** (1995) 77–82.

[10] Pateyron M., *et al.*, '3D microtomography of cancellous bone samples using synchrotron radiation', *SPIE Medical Imaging '96, Physics of Medical Imaging* **2708** (1996) 417–426.

[11] Labiche, J. C., *et al.*, 'FRELON camera: Fast readout low noise', *ESRF Newslette* **8** (25) (1996) 41–43.

[12] Salome, M., *et al.*, 'Assessment of bone micro-architecture using 3-D computed microtomography', *ESRF Newslette* (April 1997) 26–28.

[13] Castleman, K. R., 'Digital Image Processing', (Prentice-Hall, Inc., Englewood Cliffs, NJ, 1979).

[14] DIN 52-615: Bestimmung der Wasserdampf-durchlassigkeit von Bau- und Dammstoffen, 1987.

[15] Garboczi, E. J., 'Finite element and finite difference programs for computing the linear electrical and elastic properties of digital images of random materials', NISTIR 6269, U.S. Department of Commerce, 1998, also available over the Internet at http://ciks.cbt.nist.gov/garboczi.

[16] Holman, J. P., 'Heat Transfer', (McGraw-Hill, New York, 1981).

[17] Garboczi, E. J., 'Permeability, diffusivity, and microstructural parameters: A critical review', *Cem. Concr. Res.* **20** (1990) 591–601.

[18] Katz, A. J. and Thompson, A. H., *J. of Geophys. Res.* **92** (1980) 599–607.

[19] Stauffer, D. and Aharony, A. 'Introduction to Percolation Theory', 2nd. Edn. (Taylor and Francis, London, 1992).